Geocarto International
Vol. 00, No. 00, Month 2009, 1–23

ARTICLE

A local approach to optimise the scale parameter in Multiresolution Segmentation for multispectral imagery

F. Cánovas-García[a,b*] and F. Alonso-Sarría [b]

[a]*Departamento de Ingeniería Civil, Universidad Estatal de Cuenca, Av. 12 de abril, Ciudadela Universitaria, Cuenca, Ecuador*; [b]*Instituto Universitario del Agua y del Medio Ambiente, Universidad de Murcia, Edificio D Campus de Espinardo s/n 30100 Murcia, Spain*

(*XXXXXXXXX*)

The results obtained using the OBIA approach for remote sensing image analysis depend strongly on the quality of the segmentation step. In this paper, to optimise the scale parameter in a multiresolution segmentation, we analyse a high resolution image of a large and heterogeneous agricultural area.

This approach is based on using a set of agricultural plots extracted from official maps as uniform spatial units. The scale parameter is then optimised in each uniform spatial unit. Intra-object and inter-object heterogeneity measurements are used to evaluate each segmentation. To avoid subsegmentation, some oversegmentation is allowed but is attenuated in a second step using the spectral difference segmentation algorithm. The statistical distribution of the scale parameter is not equal in all land uses, indicating the soundness of this local approach.

A quantitative assessment of the results was also conducted for the different land covers. The results indicate that the spectral contrast between objects is larger with the local approach than with the global approach. This differences were statistically significant in all land uses except irrigated fruit trees and greenhouses. In the absence of subsegmentation this suggests that the objects will be placed far apart in the space of variables, even if they are very close in the physical space. This is an obvious advantage in a subsequent classification of the objects.

Keywords: Object based image analysis; Segmentation; Optimisation, *eCognition*™

*Corresponding author. Email: fulgencio.canovas@um.es

ISSN: 1010-6049 print/ISSN 1752-0762 online

DOI: 10.1080/1010604YYxxxxxxxx
http://www.informaworld.com

1. Introduction

Object Based Image Analysis (OBIA) is an alternative to the traditional pixel based approach for remote sensing image analysis. Whereas the latter is based on the statistical analysis of multispectral features of the pixels in the image, the former allows the use of a large range of additional information. Two advances are behind the expansion of this technique: the availability of high spatial resolution satellites for civil use, for example Quick Bird (Aplin *et al.* 1997); and the release of eCognition^{TM} in 2001, the first commercial OBIA software. This release has given universal access to tools previously only available in specialised research labs (Castilla and Hay 2008, Blaschke 2010).

OBIA, when used in remote sensing (GEOBIA), has been defined as a "subdiscipline of Geographic Information Science (GIScience) devoted to developing automated methods to partition remote sensing imagery into meaningful image-objects, and assessing their characteristics through spatial, spectral and temporal scales, so as to generate new geographic information in GIS-ready format" (Hay and Castilla 2008).

This approach produces better results than traditional pixel-based classification (Yan *et al.* 2006, Blumberg and Zhu 2007, Chen *et al.* 2007, Platt and Rapoza 2008, Smith 2008, Gao *et al.* 2009, Myint *et al.* 2013), especially when applied to high spatial resolution images (Yu *et al.* 2006, Lu and Weng 2007) or in regions dominated by small-scale farming (Conrad *et al.* 2010).

Additional advantages of OBIA have been highlighted (Jyothi *et al.* 2008, Lang 2008, Liua and Xiab 2010): reduces intra-class spectral variability; provides a great number of new features to characterize classes; reduces in several orders of magnitude the number of cases to process, allowing more advanced and computationally costly classification techniques to be used; and, finally, diminishes the speckled pattern in the final map. However, some disadvantages have also been identified, being the most important the dependence of the results on the quality of the segmentation step (Recio Recio 2009, Liua and Xiab 2010, Hermosilla Gómez 2011, Myint *et al.* 2013).

Therefore, it is clear that segmentation, a critical step in OBIA and specific to this technique, is the base for the extraction of real world objects (Marpu 2009). However, the perfect segmentation algorithm does not yet exists and the most widely used techniques still need to be improved (Reikik *et al.* 2007). The need for human decisions concerning the segmentation settings for each different satellite scene remains a bottleneck, allowing room for increased automatic preprocessing in GEOBIA (De Kok 2012).

Multiresolution segmentation (Baatz and Schape 2000), the segmentation algorithm used in this study, is one of the most widely used in OBIA. It has been included in *eCognition*^{TM} since 2002 (Lucieer 2004, Benz *et al.* 2004) and, despite its recent availability, it is rapidly becoming one of the most cited segmentation algorithms (Lu and Weng 2007). The key parameter for this segmentation method is the scale parameter, but there is no straightforward method to obtain an optimum value of the same. The usual approach is to find a compromise value for the whole image by trying several values and evaluating the results (Platt and Rapoza 2008, Tzotsos *et al.* 2008, Gao 2009, Conrad *et al.* 2010). However this global approach needs a certain degree of uniformity in the image, so its application to large heterogeneous images may be difficult.

The objective of this paper is to present an approach for optimising the segmentation of high resolution images, especially in large study areas, in order to obtain a land cover map for agronomic purposes. This approach is based on an empirical goodness method, which consists of quantifying some desirable segmentation properties and searching for the scale parameter that maximises them. The overall approach solves some of the problems faced

by the research in the topic:

- Instead of optimising the scale parameter for the whole image, the approach uses uniform spatial units to optimise local scale parameters. It thus uses the multi-scale aspect indirectly.
- It uses the multi-source aspect including ancillary information from a cartographic database.
- It uses the multi-method aspect since it implements several different segmentation algorithms.

For comparison purposes we also used the global optimisation method proposed in Espindola *et al.* (2006). This method is briefly explained in section 2.3.

The paper is organised as follows. In section 2 segmentation algorithms are briefly presented. In section 3 we describe the study area and the input information that was used. The proposed approach is outlined in section 4. In section 5, the main results are presented and discussed. Finally, the last section offers some conclusions.

2. Segmentation algorithms

There is a wealth of literature on the different segmentation approaches. The most relevant approaches in remote sensing are:

- Algorithms based on unsupervised classification, like *k-means* and *isodata*.
- Algorithms based on edge detection search for the pixels corresponding to the limits of the real elements in the landscape and use them as object boundaries.
- Algorithms based on region growing include algorithms that merge pixels recursively from an initial set of pixels acting as seeds. These seeds are distributed through the image according to previously established criteria.

2.1. *Multiresolution Segmentation*

The multiresolution segmentation algorithm is based on region growing. The details of the algorithm can be consulted in Baatz and Schape (2000), where the authors claim that the objects of interest typically appear simultaneously on different scales in an image; therefore, the scale used for the extraction of objects should be adaptable to fit the size of the objects.

The first step in the application of this algorithm is to consider each pixel in the image as an object; thus the seed pixels are seed objects. Each possible fusion of a seed object (i) with one of its neighbouring objects (j) means an increase in heterogeneity ΔH_{ij}. Only those fusions with a ΔH_{ij} smaller than a previously established threshold (SP) are considered. If an object i is surrounded by any object j with $\Delta H_{ij} < SP$, a heuristic decision rule must be applied to decide whether any of them should be merged with i. The process continues iteratively until there are no more possible fusions. A low threshold allows a lower number of fusions, resulting in a larger number of smaller objects. In contrast, a large threshold will produce a small number of larger objects. This is why this threshold is called the scale parameter (SP).

The process requires two key elements: (1) that the definition of object heterogeneity should allow ΔH_{ij} to be calculated for the merging of a pair of objects (i and j); (2) that a heuristic decision rule should decide which objects will be merged in each step.

The increase in heterogeneity after a fusion of two objects, i and j, is calculated as a linear combination of the increases in spectral and shape heterogeneities (Gao 2009):

$$\Delta H_{ij} = w_h \cdot \Delta Hspc_{ij} + (1 - w_h) \cdot \Delta Hshp_{ij} \quad (1)$$

where w_h is a weighting coefficient to give more importance to one of the heterogeneities, and ij represents the object resulting from merging objects i and j.

Spectral heterogeneity ($Hspc_{i,d}$) for an object (i) and a spectral band (d) can be approximated by the variance or standard deviation of their values and the increase in spectral heterogeneity (Baatz and Schape 2000):

$$\Delta Hspc_{ij} = \sum_d w_d[a_i \cdot (Hspc_{ij,d} - Hspc_{i,d}) + a_j \cdot (Hspc_{ij,d} - Hspc_{j,d})] \quad (2)$$

where $Hspc_{i,d}$ and $Hspc_{j,d}$ are the the spectral heterogeneities of band d in two neighbour objects that are candidates for merging; $Hspc_{ij,d}$ is the heterogeneity in band d of the object resulting from the fusion; a_i and a_j are the sizes of both objects; and, finally, w_d is a weighting coefficient for each band.

Shape heterogeneity for an object ($\Delta Hshp_{ij}$) is calcuated as a weighted average of compactness and smoothness, as defined in Baatz and Schape (2000) or Gao (2009). In this study, a value of 0.5 was used for both weighting factors.

Once the increase in heterogeneity resulting from each possible merging of an object with its neighbours has been calculated, the heuristic decision rule is used to decide which of the neighbour objects with $\Delta H_{ij} < SP$ is more suitable for merging with the object analysed. The multiresolution segmentation algorithm uses a heuristic called "more adequate, local and mutual" (Baatz and Schape 2000), which:

(1) finds for object i, the adjacent object j with lowest ΔH_{ij}
(2) finds for j, the adjacent object k with lower ΔH_{jk}
(3) confirms that i=k; if not, the same cycle is repeated with j.

2.2. *Spectral Difference Segmentation*

The objects resulting from a multiresolution segmentation do not correspond to real elements in the landscape and are called primitive objects (DEFINIENS 2004, Benz *et al.* 2004, DEFINIENS 2008). They are usually smaller than objects produced by manual digitising (Corcoran *et al.* 2010), which is why it is difficult to compare both segmentation approaches.

Multiresolution segmentation is appropriate for finding primitive objects, but there is a need for other fusion algorithms to merge those primitive objects into a set of larger objects that are more related to landscape elements (Benz *et al.* 2004, Yan *et al.* 2006).

Spectral difference segmentation is one of the most frequently used fusion algorithms in *eCognition*$^{\text{TM}}$ and several authors have used it to refine segmentation results (Esch *et al.* 2008, Zabala *et al.* 2010, Johnson and Xie 2011). This algorithm improves the spatial correspondence between primitive objects and landscape elements, reducing the number of objects. It merges two objects if the difference between the average value of their features is lower than a threshold called the maximum spectral difference (MSD):

$$SD_{ij} = \sum_{d} w_d \cdot |m_{i,d} - m_{j,d}| \tag{3}$$

where $m_{i,d}$ and $m_{j,d}$ are the averages for band d calculated for two objects, and w_d is the band weight, according to its importance. If $SD_{ij} < MSD$, the fusion is allowed.

2.3. *Validation and optimization of segmentation*

One of the main problems with OBIA, particularly with the multiresolution segmentation algorithm, is the impossibility of knowing *a priori* the most suitable set of parameters for delimiting the objects (Espindola *et al.* 2006, Lu and Weng 2007, Tian and Chen 2007, Walker and Blaschke 2008, Gao 2009). Another problem is the validation and optimisation of the parameters. Usually, a very time-costly trial-error approach is used, but does not guarantee an optimal result (Schiewe 2002, Espindola *et al.* 2006, Tian and Chen 2007, Nussbaum and Menz 2008, Platt and Rapoza 2008, Costa *et al.* 2008, Kim *et al.* 2008, Walker and Blaschke 2008, Marpu 2009, Gao 2009, Dragut *et al.* 2010, Gao *et al.* 2011, Rosa and Stow 2014). Moreover, this approach is usually applied to the complete image, and a compromise scale parameter is obtained for the image as a whole, which does not necessarily work for the different plots.

The methods used to validate the results were classified in Zhang (1996). Although this classification was not initially intended to be used with remote sensing imagery, it is essentially valid and has been accepted (Schiewe 2002, Castilla Castellano 2003, Espindola *et al.* 2006, Costa *et al.* 2008, Radoux and Defourny 2008, Neubert *et al.* 2008, Marpu 2009). Segmentation results can be evaluated in an analytical or empirical form (Zhang 1996). The first way is based on an *a priori* examination of the algorithm, its principles and properties. When applying the empirical approach there are two options:

- Empirical discrepancy methods: The automatic segmentation is compared with another digitised by a photointerpreter, which is considered as ground-truth, and the differences are quantified. These methods are mostly used in OBIA when the aim is to validate one or several segmentations (Delves *et al.* 1992, Neubert and Meinel 2003, Lucieer 2004, Carleer *et al.* 2005, Zhang *et al.* 2005, Radoux and Defourny 2007, Tian and Chen 2007, Möller *et al.* 2007, Neubert *et al.* 2008, Neubert and Herold 2008, Schöpfer *et al.* 2008, Fu *et al.* 2013). However, as is claimed in (Zhang *et al.* 2005), manually digitising a reference image is difficult, subjective, and time-consuming; furthermore, it would be impossible to choose the better of two different, skillful manual segmentations. Thus, empirical discrepancy methods are difficult to use when the goal is optimisation.
- Empirical goodness methods: The objective is to quantify any *a priori* desirable segmentation property, the segmentation with the best results is considered the most appropriate. There is no need for a reference image and the method is easy to use in optimisation. This is the approach used in this study.

Some approaches focus on internal homogeneity measurements (Dragut *et al.* 2010) based on local variability increments that arise in different segmentations obtained with increasing values of the scale parameter. These ideas are based on Woodcock and Strahler (1987), who established the existing relations between the spatial structure of the image, the dimensions of real world objects, and the spatial resolution of the image.

Espindola *et al.* (2006) integrates both internal homogeneity and external heterogeneity criteria to measure segmentation quality using an objective-function. External heterogeneity is measured as the spatial autocorrelation. The rationale is that a segmentation should have two basic properties: (1) the resulting objects are internally homogeneous; (2) the resulting objects are different from those nearby.

The objective function used by Espindola *et al.* (2006) combines external heterogeneity and internal homogeneity measurements. The first measurement is the Moran autocorrelation index (Fotheringham *et al.* 2000), calculated, for each band, from the objects's average values for that band. The second one is a size-weighted variability index, which is also calculated for each band. This is based on the object internal variance (equation 4):

$$v_d = \frac{\sum_{i=1}^{N} a_i \cdot S_{di}^2}{\sum_{i=1}^{N} a_i} \tag{4}$$

where v_d is the internal homogeneity in band d, S_{di} is the variance of each object (i) for each band (d), a_i the size of object i and N the number of objects. This measurement guarantee that all polygons in the image contribute equally to the calculation of the parameter, preventing instabilities resulting from a high number of small areas.

As far as we know, little work has been done on the selection of objective functions to maximise internal homogeneity and external heterogeneity. However, one of the most relevant works in this respect is Espindola *et al.* (2006) which proposes two functions to normalise both internal homogeneity and external heterogeneity to values between 0 and 1; the sum of both functions is the measure to be maximised. Other authors embrace this equation with some modifications or deal with the problem with similar statistics (Johnson and Xie 2011). This proposal has been used successfully by Zhang and Xie (2014).

3. Study area and data set

The study area (Figure 1) is located in the Murcia Region in south-east Spain, and corresponds to Irrigation Unit (UDA) 28, as defined by the River Segura Basin Hydrological Plan, the in-force water resources planning law passed on 24 July 1998 (R.D. 1664/1998). A 150 m buffer zone has been added to guarantee the complete inclusion of the relevant plots. The area is centered at X=600000,Y=42175000 (UTM 30N), equivalent to latitude=$38^o05'50''N$ and longitude=$1^o51'35''W$, both coordinate pairs based on the ETRS89 datum. Including the buffer, it has an area of 9,070 ha. Most of it, except 600 ha, is included in the basin of the River Argos. This river is a tributary of the River Segura, a typical semiarid river.

Most of the information used in this research was obtained from the Environmental Integration and Management Service (SIGA), a branch of the CARM government. The data, obtained under the Natmur-08 project (CARM 2009), consist of a 2 m resolution multispectral (Blue, Green, Red and Near Infrared) image, a 0.45 m panchromatic digital image, and a 4 m resolution DEM interpolated from LIDAR points. The images corresponding to the study area were acquired on 9,10 and 11 July 2008 with an Intergraph Z/I-Imaging Digital Mapping Camera. The final 0.45 m resolution multispectral image

was obtained using Gram-Schmidt fusion (Clayton 1971, Farebrother 1974, Cánovas-García and Alonso-Sarría 2014) as previous treatment. This final image was used in this study.

4. Methodology

The main aim of this study was to optimise the scale parameter used with the multiresolution segmentation algorithm. Due to the lack of *a priori* valid criteria to identify the optimal segmentation parameters, a procedure to extract primitive objects using the multiresolution segmentation algorithm is proposed. This is based on the execution of several segmentations and their statistical analysis. From these analyses, and using criteria that will be defined later, a general decision rule can be obtained. This rule identifies which scale parameter maximises the empirical properties characteristic of good segmentation in the context of an empirical goodness method.

The approach follows that used in Espindola *et al.* (2006) with some modifications to provide better results given the large size and heterogeneity of the study area. In short, the difference is that external heterogeneity was calculated using the Geary coefficient rather than Moran's coeeficient because the former allows the variability of the objects to be taken into account. The most relevant difference from most other OBIA-related studies, is that, instead of a global (the whole image) approach, we take a local (uniform spatial units) approach. Another important difference is the optimization of the scale parameter, which is discussed further in this section.

4.1. *Extraction of primitive objects: Internal homogeneity and external heterogeneity measurements*

The ideal situation would be to find a set of parameters that maximises internal homogeneity and reduces external heterogeneity. However, in most cases, the two functions are inversely proportional, and a graphical approach can be used.

Following Baatz and Schape (2000) and Espindola *et al.* (2006), equation 4 is used in our work as the internal homogeneity measurement. However, we used the Geary coefficient (Geary 1954) as the external heterogeneity statistic, rather than the Moran autocorrelation index. The original formulation of the Geary index can be expressed for any feature as:

$$c = \frac{N-1}{2 \cdot \sum_i^N \sum_j^J w_{ij}} \cdot \frac{\sum_i^N \sum_j^J w_{ij} \cdot (x_i - x_j)^2}{\sum_i^N (x_i - \mu_x)^2} \tag{5}$$

where N is the number of objects obtained in each uniform spatial unit, x_i is the value of the feature in object i, x_j is the value of the feature in one of the J objects surrounding object i, μ_x is the average of feature x, and w_{ij} is 1 if both i and j share an arc, and 0 otherwise. If c is smaller than one, it indicates a negative spatial autocorrelation; if c is larger than one, the autocorrelation is positive; finally, if $c = 1$ there is no autocorrelation.

The formulation of the Geary coefficient has been modified in this study by substituting the difference values $(x_i - x_j)$ for an Euclidean distance between both objects in a 2-dimensional space defined by the average and the standard deviation of the band in each object:

$$D_{ij} = \sqrt{(m_i - m_j)^2 + (s_i - s_j)^2} \tag{6}$$

We believe that, by including objects variability, this distance between objects allows a more complete characterization of the differences between two objects. In fact, the possibility of using this form of Euclidean distance is why we used the Geary index instead of the Moran index as proposed in Espindola *et al.* (2006). Hence, the Geary coefficient applied was:

$$c = \frac{N-1}{2 \cdot \sum_i^N \sum_j^J w_{ij}} \cdot \frac{\sum_i^N \sum_j^J w_{ij} \cdot D_{ij}^2}{\sum_i^N D_{i\mu}^2} \tag{7}$$

where:

$$D_{i\mu} = \sqrt{\left(m_i - \frac{\sum_{h=1}^H m_h}{H}\right)^2 + \left(s_i - \frac{\sum_{h=1}^H s_h}{H}\right)^2} \tag{8}$$

where H is the number of objects in the image.

The modification of the Geary coefficient introduced in this work is the transformation of w_{ij} from a Boolean variable (contiguity or non-contiguity) into a percentage of contiguity:

$$w_{ij} = 100 \cdot \frac{P_{ij}}{P_i} \tag{9}$$

where P_i is the perimeter of object i and P_{ij} the perimeter shared by objects i and j.

4.2. *Uniform spatial units*

The validity of internal homogeneity and external heterogeneity criteria to optimise the scale parameter depends heavily on having a uniform study area for the scale parameter to be representative of the whole area. The study area also needs to be large enough for the algorithm to be executed. The study area in this research is large, at least compared with the areas analysed in other OBIA studies (Carleer *et al.* 2005, Chen *et al.* 2006, Espindola *et al.* 2006, Tian and Chen 2007, Esch *et al.* 2008, Corcoran *et al.* 2010, Dragut *et al.* 2010, Johnson and Xie 2011, Fu *et al.* 2013), and contains several different land uses. This is why the global approach to optimise the scale parameter was not considered suitable opting, instead, for a local optimisation approach.

The searching and manual digitising of uniform spatial units would have been almost impossible for such a large area and would run counter to the idea of having a semiautomatic segmentation procedure. Not to mention the difficulty of defining and measuring a uniformity index. As a result, we decided to use a land use map to obtain agricultural plots to be used as uniform spatial units. After an analysis of the available digital land use maps in the Spanish official cartography, the Agricultural Plots Geographic Information

System (SIGPAC) cartography, with a nominal scale of at least 1:10,000, was selected as the most appropriate source to obtain uniform spatial units. A detailed description of this map can be found in Recio Recio (2009). We are assuming that each agricultural plot in this ancillary layer is, if not completely uniform, at least more uniform than the study area as a whole. Figures 5 to 10 depict some of the analysed uniform spatial units showing, at least qualitatively, a high degree of uniformity.

SIGPAC should not be considered a proper land use layer. Only crops eligible for subsidies are identified and labelled in the map; moreover, the map shows the land uses declared by the owners, not always a reflection of reality; finally, the updates rely on the owners' declarations. Although, its geometry is fairly reliable, it is not error-free, which is why some time had to be devoted to editing topological inconsistencies of the layer and to merging agricultural plots with the same cover. Less frequently, some plots had to be divided to maintain just one cover in each plot. As a result of such editing the number of plots in the SIGPAC ancillary layer was reduced from 21,400 to 9,582.

The SIGPAC layer was then used just to obtain the boundaries of the homogeneous cover plots, while the registered land use was not taken into account. The method we propose therefore is not sensitive to the degree of updating of this layer.

4.3. *The objective functions*

The first step in defining the objective functions was to linearly transform both the heterogeneity (c_d) and the homogeneity (v_d) functions for each band (d) (equations 10 and 11). To combine both curves a third one, $F(v_d, c_d)$ was calculated (equation 12).

$$F(v_d) = \frac{max(v_d) - v_{jd}}{max(v_d) - min(v_d)} \tag{10}$$

$$F(c_d) = \frac{min(c_d) - c_{jd}}{min(v_d) - max(c_d)} \tag{11}$$

$$F(v_d, c_d) = \frac{F(v_d) + F(c_d)}{2} \tag{12}$$

The purpose of these transformations was to keep the values within the range 0-1 with the higher values indicating the fulfilment of the desired properties (i.e. high external heterogeneity and high internal homogeneity).

The multiresolution segmentation algorithm was used with 3 spectral bands (red, green, and near infrared). The importance of shape homogeneity was 30% and the weighting coefficient for both compactness and smoothness was 50%.

If we let the three parameters vary in order to find the best combination, the number of possible combinations would not be feasible from a computational point of view. Therefore, we decided to optimise the segmentation by varying the most critical parameter, the scale parameter, fixing the importance of shape homogeneity at 0.3 and the smoothness and compactness weights to 0.5. The scale parameter was allowed to vary from a value that was seen to produce oversegmentation (75) to another that produced a strong subsegmentation (1025), with steps that were small enough to ensure minimal

changes from one step to the other (25). However, these values may not be generalizable to other images, since they could depend on the radiometric resolution of the sensor.

The authors of the algorithm Baatz and Schape (2000) consider that the spectral criterion is more relevant than the shape criterion, so they recommend using a value smaller than 0.5 as the importance of shape heterogeneity. In many OBIA-related papers the usual values range between 0.1 and 0.4 (Al-Khudhairy *et al.* 2005, Walker and Blaschke 2008, Zhou *et al.* 2009). So we considered a value of 0.3 as acceptable.

The 9,582 uniform spatial units were analysed, creating $F(v_d)$ and $F(c_d)$ and $F(v_d, c_d)$ for each band and plot. Figures 5 to 8 show four examples of the relation of such curves with the scale parameter.

A strong inverse correlation between $F(v_d)$ and the scale parameter is evident from the curves. From the observation of several curves, it can be stated that such smooth behaviour is usual in homogeneous large plots. The $F(c_d)$ function provides more information: as a general pattern, $F(c_d)$ is small for a very small SP, increasing with it until a threshold is reached, at which point the curve tends to flatten out. Additionally, there is a relation between the evolution of $F(c_d)$ and the spatial structure of the image, more specifically the presence or absence of different elements inside a uniform spatial unit (trees, bare soil, buildings, etc.).

Some preliminary tests were carried out to evaluate the result of using the maximum $F(v_d, c_d)$ criterion to obtain the scale parameter. In some cases this function was an almost horizontal line (Figure 8); moreover, using the smallest SP at which the maximum value of $F(v_d, c_d)$ was reached did not produce good results.

However, our hypothesis was still that valid criteria for any kind of land cover could be extracted from the curves. It is clear that internal homogeneity and external heterogeneity are two inversely correlated objectives; when SP is low, $F(v_d)$ is high and $F(c_d)$ is low, while the opposite occurs when SP is high.

It was therefore decided to consider the SP value at which the two curves intersect as a trade-off between both objectives and, consequently, as the optimum SP. Because the whole process was carried out with three bands, the minimum SP value obtained in any of them was considered the final optimum SP. The minimum was preferred to the mean in order to provide a more conservative estimation to avoid subsegmentation of the homogeneous plots.

4.4. *Improvement of the spatial correspondence of the primitive objects*

The spectral difference segmentation algorithm was used to modify the primitive objects in order to improve their spatial correspondence with the real landscape objects. The inputs for this algorithm are (1) the maximum spectral difference (MSD) value for use as a threshold, and (2) the bands in which the method is to be applied. In this case, the bands are the same as those used with the multiresolution segmentation algorithm. In order to obtain an objective procedure to chose the optimum MSD for each uniform spatial unit, several values were tested in several uniform spatial units. The results showed that MSD increases with SP, following a curve defined by equation 13.

$$MSD(SP) = \begin{cases} 1500, & if\ SP >= 600; \\ 1500 \cdot (1.5 \cdot \frac{SP}{600} - 0.5 \cdot \frac{SP}{600}^3), & if\ SP < 600; \end{cases} \quad (13)$$

4.5. *Segmentation quality*

The use of digitised objects as a reference to validate a segmentation has been limited, as far a we know, to the use of very few objects in very small study areas (Lucieer and Stein 2002, Neubert and Meinel 2003, Liua and Xiab 2010, Johnson and Xie 2011). Having a set of digitised objects large enough to be representative increase substantially the complexity of the study, especially in large study areas, as it is the case for this study.

Following Zhang (1996) and Zhang *et al.* (2008), an evaluation based on an empirical goodness method, as the one used in this study, relies only on the segmented image, without comparison with a manually-digitised reference set of objects. The optimisation of the segmentation parameter is considered enough to obtain the best possible segmentation. This approach has been widely accepted among OBIA researchers (Schiewe 2002, Espindola *et al.* 2006, Costa *et al.* 2008, Neubert and Herold 2008, Radoux and Defourny 2008, Dragut *et al.* 2010).

However, in order to have a more quantitative and objective quality measurement, two statistical analyses were carried out. The set of uniform spatial units was randomly sampled to obtain 50 uniform spatial units in each land use, except "seedlings" that included just 15 units. The class of each uniform spatial unit was assigned during a field work campaign. The distribution of the scale parameters obtained using the local approach was used to verify that differences in the scale parameter among different land uses exist and can be related to their spatial patterns. Kruskal–Wallis one-way analysis of variance using ranks was used to decide whether the population distributions are identical. Fisher exact test was then used to compare the distributions of the scale parameter in every pair of classes searching for significantly different pairs.

On the other hand, a simple measure of the quality of each method has been introduced. In the absence of subsegmentation, a segmentation is better than another if, for any band, the reflectivity of the pixels in an object is different to that of the surrounding objects. The arithmetic mean of the absolute differences between each object and its neighbours can measure this property:

$$\mathrm{Diff}_i = \frac{\sum_{j \in J} w_{ij} |m_i - m_j|}{|J|} \tag{14}$$

where i is the object being measured, j is each of the objects contiguous to i, m_i the pixel average of object i, m_j the pixel average in object j, w_{ij} a percentage of contiguity (indicated in equation 9), J is the set of the objects that share a boundary with i, and $|J|$ is the number of members in J.

The values of Diff obtained with the global and local approaches were compared for each class. To take into account the size of each object, avoiding at the same time the computational and statistical problems of having a huge number of cases, 5,000 pixels were selected from each class. Each object contributed to this amount with a number of pixels proportional to its size. These pixels were used to build the density function of Diff, calculate the medians, and compare the medians obtained with the global and local approaches using the Mann–Whitney U test to determine in which classes the medians were significantly different. We used a non-parametric test because, as can be seen in figure 4, the distributions are far from normal. On the other hand, except for irrigated cereal and arable land, the distributions obtained using both global and local approaches are very similar, with the same variance. Consequently, the conditions to apply Mann–

Whitney U test are fulfilled except for those two land uses whose medians are clearly different just seeing the density distributions.

4.6. *Work flow*

Figure 2 shows a diagram with the whole work flow. The first step was to calculate the internal homogeneity and external heterogeneity statistics in the three bands used to segmentate each plot with each scale parameter. The *eCognition*$^{\text{TM}}$ software was used to make all the segmentations for all the uniform spatial units, as defined by the SIGPAC map. The segmentations were carried out using variable SP values, ranging from 75 to 1025 with steps of 25. Segmentation was hierarchical, which means that segmentations using higher SP values used the information obtained in the lower SP segmentations. In this way, the whole set of segmentations can be completed in a reasonable time. The algorithm was forced to keep to the SIGPAC plot boundaries, which means that two objects included in different uniform spatial units were not merged even if they fulfilled the heterogeneity criteria; this is a feature included in *eCognition*$^{\text{TM}}$ software. Finally, the statistics were calculated for all objects within a plot, for all the plots and for each scale parameter. Although this is a slow process, the possibility of creating sequential rulesets in *eCognition*$^{\text{TM}}$ is very useful.

This process created a large amount of text files containing the statistics, which were exported into R software (R Development Core Team 2009). This software was used to build the curves and to locate the intersection points, that is, the lowest SP value which produced a change in the sign of the function $F(v_d)$ - $F(c_d)$. Once the optimum SP values had been obtained for each plot, they were used again in *eCognition*$^{\text{TM}}$ to make the final segmentation of the corresponding plots.

Finally, and also in *eCognition*$^{\text{TM}}$ the spectral difference segmentation algorithm was applied to all the plots.

The boundaries of the agricultural plots were, once again, maintained, meaning that if two objects (i and j) were located in different plots, they were not merged even if $SD_{ij} < MDS$. The values of SD_{ij} were calculated using equation 3.

The method in Espindola *et al.* (2006) was also applied to the red band, using different scale parameters from 75 to 1025 with steps of 25. The importance of the shape criterion was established at 30%.

We used the same parameters as in the previous case to obtain results that could be compared.

Our method is very time-consuming, taking in our case about 15 hours of computation in a 64-bit multicore (8 core) server with 12 GB RAM.

5. Results and discussion

Figure 3 and table 1 show the scale parameter distribution and medians in different land uses. The lower median values of SP appear in seedlings and irrigated fruit trees (250), while irrigated cereals (375) is the land cover with larger value. Arable land, olive trees, and greenhouses (350) were also segmented with high SP values. In general, plots with tree crops have lower scale parameters than those with non-tree crops because smaller objects have to be identified in the former. Tree crops show also a lower dispersion in SP values with higher density peaks, while non-tree covers show larger dispersion. The reason is that non-tree covers represent large areas whose pixels have similar and spatially

non-autocorrelated reflectivity, so they are prone to be randomly oversegmented. This oversegmentation is easily solved in the post-segmentation step but produces a large dispersion in the scale parameter values. Some cases of bimodality appears, specially in rainfed cereals. The reason might be some differences in cultural techniques.

The results of the Kruskal–Wallis test showed that scale parameter do not have the same distribution in at least a pair of classes (p-value=0.0000325). Table 1 shows the p-values of the Fisher exact test conducted to compare the distributions of each pair of classes. There is a subset of four land covers for which it cannot be rejected that their spatial parameter distributions are the same: Irrigated cereal, arable land, olive trees, and greenhouses. In the case of almond trees, the same distribution hypothesis cannot be rejected with arable land and olive trees. In the case of rainfed cereal, this hypothesis cannot be rejected with irrigated cereal, irrigated fruit trees, olive trees, and greenhouses. On the other hand, the distribution of scale parameter for seedlings is different to all the other land uses.

The differences in median among land uses, the differences in density functions, and the fact that the dispersion by class is lower than overall dispersion suggest that the local approach can produce a better segmentation than the global, giving to each spatial unit an adequate value.

Figure 4 show the distribution of Diff, both for the local and global methods, and for all land uses; table 2 shows the median values. Diff is always higher when using the local approach than when using the global approach. The p-values of the Mann–Whitney U test are highly significant except for greenhouses and irrigated fruit trees. In the land covers where the fulfilment of the conditions to use the Mann–Whitney U test are less clear (arable land and irrigated cereals) the difference between global and local approaches are clear form the density distributions (Figure 4). So, assuming no subsegmentation, the local optimisation method offer better contrast among neighbouring objects (except for arable land and irrigated cereals). According to a visual inspection of the results, none of the two approaches has produced subsegmentation in any land cover except in the case of seedlings. In this case the local optimisation method subsegments 5 of the 15 analysed plots, while the global optimisation do it in 6.

Figures 5 to 8 show some examples of the obtained segmentations in uniform spatial units. Figure 5 shows a uniform spatial unit with seedlings. This is an example of how the proposed method allows very small objects to be identified if the required conditions (a large enough plot and a good enough spectral contrast between objects) are met. The optimal scale parameter identified for this spatial unit (125) have properly delimited even small seedlings. However the plot is divided into many objects, most of them very similar, although by applying the second segmentation algorithm, Spectral Difference Segmentation, the number of objects, including background bare soil, is much reduced. On the contrary, the global scale parameter (310), although it may be optimal for the overall image, subsegmented this unit.

In other cases, both local and global approaches have produced similar results. Figures 6 and 7 show two examples where large trees are properly identified as separate objects, and Figure 8 shows an example in a ploughed plot. Both in Figure 7 and Figure 8 the application of the Spectral Difference Segmentation algorithm favours the generation of large, homogeneous objects preventing subsegmentation.

Some examples of the segmentation results in different plots are presented in Figures 9 and 10 to discuss some qualitative aspects of the results in the main land uses present in the study area. The aim of segmentation is to extract primitive objects that do not usually have an exact correspondence with real landscape elements. However, these primitive

objects should maintain some important properties, such as as low spectral variance, similar sizes for the different objects included in the same land cover, and absence of subsegmentation.

Figure 9 (a and b) shows two almond tree plots. Image a is a small plot, which is a disadvantage when applying our method, although the result is acceptable. The trees remain separated from the surrounding bare soil. Although the delimitation of the trees is not very clear and some small bare soil patches are included within the tree objects, there are no split trees, a very common problem when using a compromise scale parameter. Such separation occurs when the shadow of the tree appears next to the tree. In this case, two objects are often created: the illuminated part of the tree and the shadow merged with the darkest part of the tree. Image b shows a similar result in a larger plot.

The two cereal plots in Figure 9 (c and d) are segmented in a way characteristic of cereal plots where the stubble remains in the plot. A distinctive pattern of alternating stripes of cut flush cereal and stubble appears. For this reason, although the land cover is the same, these plots include several different long and narrow primitive objects. Even using high scale parameters, these objects do not merge, due to the large differences in their reflectivity. In image c, the contrast is less clear, which results in larger primitive objects, even when a smaller scale parameter is applied.

Plots with irrigated fruit trees (Figure 9 e and f) are very heterogeneous because of the different tree sizes. As long as there is no intersection between the canopies and the bare soil surface between trees has no vegetation, the high contrast between canopy and bare soil allows good differentiation of the former. However, some trees (for example peach trees), due to the time of the year when the image was taken, show very developed canopies without gaps between them. As a consequence, it is impossible to separate individual trees and the quality of the segmentations is variable. Arable land (Figure 10 a and b), just like irrigated grass crops or wasteland, forms large objects due to the high spectral homogeneity that characterises this cover, producing good segmentation.

Figure 10 (c and d) shows an olive trees plot. Olive trees are usually easy to differentiate from the bare soil underneath. As with other tree covers, the success of the segmentation depends on the reflectivity of the bare soil, which is related with the agricultural practices carried out. If there is another crop in the soil underneath, or a dense cover of weeds the results are worse. Figure 10 e and f show a plot covered with greenhouses. Being quite different from other covers, greenhouses are usually very well segmentated. They are also isolated constructions within agricultural plots, so the probability of merging with a different kind of building is negligible.

In general, the results of the proposed approach can be considered quite satisfactory. Land covers belonging to different kinds of crops appear in different objects. There is a tendency to oversegmentation, but not to subsegmentation; however, this is not a problem because oversegmentation can be easily handled in further steps of the classification process. Several errors, however, have been identified, belonging to three main types:

- Errors due to the properties of the images. Some objects were not properly identified because they were too small for the spatial resolution of the image or, less importantly, too similar to the neighbouring objects for the radiometric resolution.
- Errors due to the structure of the agrarian landscape. The results were less accurate in areas with small and congested plots. Another relevant factor is the attention given to agricultural practices. In general, properly managed plots are easier to segmentate, while abandoned plots are characterized by a mixture of non vigorous trees and seasonal weeds that are easily merged.
- Some problems arise from the characteristics of the method. Using uniform spatial

units introduces artificial boundaries. Another problem is the strong sensitivity of the whole approach to the quality of the vector map used to support the segmentation. It is crucial that the plots should be uniform, and large enough compared with the image resolution.

6. Conclusions

In this study, a local approach using uniform spatial units is used to optimise the scale parameter when applying the multiresolution segmentation algorithm to a high resolution image of a large and heterogeneous agricultural area. The empirical goodness method to validate the segmentation results was easily adapted to search for an optimal segmentation, especially compared with the empirical discrepancy methods. In light of the results, we consider it an acceptable starting point for use in multiresolution segmentation in an OBIA remote sensing analysis.

The rationale for such a local approach is that in large and dissimilar images, a global optimisation of the scale parameter produces inappropriate values for some of the diverse land covers included in the image. In contrast, the local approach allows application of different heterogeneity criteria to different land covers providing an optimum scale parameter for each uniform spatial unit.

Despite the amount of segmentations necessary (39 segmentations in each of the 9,583 uniform spatial units) both the programming capabilities of R and the sequential rulesets available in *eCognition*^{TM} allow the work flow to be organised in an efficient, semi-automatic way without much difficulty.

The statistical distribution of the scale parameter is not equal in all land uses, indicating the soundness of this local approach in such a large and diverse study area. However, the hypothesis of having the same distribution could not be rejected for some pairs of classes.

A qualitative evaluation suggests that the results are quite satisfactory. Noteworthy is the good segmentation obtained for tree covers, whose correct segmentation is usually very difficult when using a global scale parameter. However, some problems were identified in the segmentation of certain land covers, most related with the very low spectral contrast between some real elements and their neighbouring elements. When this happens segmentation is very difficult regardless of the method used.

We also carried out a quantitative assessment of the results, for the different land covers, using relatively simple statistics. The results indicate that the spectral contrast between objects is larger with the local approach than with the global approach. This differences were statistically significant in all land uses except irrigated fruit trees and greenhouses. In the absence of subsegmentation, as was mostly the case, this suggests that the objects will be placed far apart in the space of variables, even if they are very close in the physical space. This is an obvious advantage in a subsequent classification of the objects.

The multiresolution segmentation algorithm is not particularly suitable for generating objects which can be compared with those obtained by manual delineation of the coverages. In contrast, the integration of different algorithms using the Cognition Network Language (CNL) and *eCognition*^{TM} software (in which the former is implemented) may produce a segmentation in which the objects generated are more related with real landscape elements. The reason is that *eCognition*^{TM} includes tools to integrate the elements necessary to carry out a flexible classification-based segmentation.

Interpretation of the internal homogeneity and external heterogeneity curves can be useful for locating the optimal scale parameter in each homogeneous plot. However, neither is able to identify the optimum segmentation without the other. It would be interesting to devote more effort to studying their behaviour in different types of land cover because it is possible that the $F(c_d)$ curves could even be used as landscape structure signatures to characterise different land covers.

Acknowledgements

This study was carried out within the framework of 15233/PI/10, funded by Fundación Séneca. We would like to thank the CARM Environmental Integration and Management Service (SIGA) for providing us with the imagery of our study area and the General Direction of the Common Agriculture Policy (CARM agricultural authority) for providing us with the SIGPAC data. This research has been also partly funded by Prometeo Project, Secretariat of Higher Education, Science, Technology and Innovation, Gobierno de Ecuador.

We also thank the two anonymous reviewers whose suggestions have substantially improved this manuscript.

Conflicts of Interest

The authors declare no conflicts of interest.

References

Al-Khudhairy, D., Caravaggi, I., and Giada, S., 2005. Structural Damage Assessments from Ikonos Data Using Detection, Object-Oriented Segmentation, and Classification Techniques. *Photogrammetric Engineering & Remote Sensing*, 71 (7), 825–837.

Aplin, P., Atkinson, P., and Curran, P., 1997. Fine spatial resolution satellite sensors for the next decade. *International Journal of Remote Sensing*, 18 (18), 3873–3881.

Baatz, M. and Schape, A., 2000. Multi-resolution Segmentation: an optimization approach for high quality multi-scale image segmentation. *In*: J. Strobl, T. Blaschke and G. Griesebner, eds. *Angewandte Geographische Informationsverarbeitung XIII*. Wichmann Verlag, 12–23.

Benz, U., *et al.*, 2004. Multi-resolution, object-oriented fuzzy analysis of remote sensing data for GIS-ready information. *ISPRS Journal of Photogrammetry & Remote Sensing*, 58, 239–258.

Blaschke, T., 2010. Object based image analysis for remote sensing. *ISPRS Journal of Photogrammetry and Remote Sensing*, 65, 2–16.

Blumberg, D. and Zhu, G., 2007. Using a hierarchical multi-resolution mechanism for the classification and semantic extraction of landuse maps for Beer-Sheva, Israel. *International Journal of Remote Sensing*, 28 (15), 3273–3289.

Cánovas-García, F. and Alonso-Sarría, F., 2014. Comparación de técnicas de fusión en imágenes de alta resolución espacial. *geofocus*, (14), 144–162.

Carleer, A., Debeir, O., and Wolff, E., 2005. Assessment of Very High Spatial Resolution Satellite Image Segmentations. *Photogrametric Engineering & Remote Sensinsg*, 71-11, 1285–1294.

CARM, 2009. *Proyecto NATMUR-08: Vuelo fotogramétrico y levantamiento LIDARde la Región de Murcia* [online]. : . Tech. Report [1 July 2010].

Castilla, G. and Hay, G., 2008. Image objects and geographic objects. *In*: T. Blaschke, S. Lang and G. Hay, eds. *Object-Based Image Analysis. Spatial Concepts for Knowledge-Driven Remote Sensing Applications*. Springer, 91–110.

Castilla Castellano, G., 2003. Object-oreinted Analysis of Remote Sensing Images for Land Cover Mapping: Conceptual Foundations and Segmentation Method to Derive a Baseline Partition for Classification. Thesis (PhD). Universidad Politécnica de Madrid.

Chen, I., *et al.*, 2007. Object-oriented classification for urban land cover mapping with ASTER imagery. *International Journal of Remote Sensing*, 28 (20), 4645–4651.

Chen, J., Pan, D., and Mao.Z., 2006. Optimum segmentation of simple objects in high-resolution remote sensing imagery in coastal areas. *Science in China Series D: Earth Sciences*, 49 (11), 1195–1203.

Clayton, D., 1971. Algorithm AS 46: Gram-Schmidt Orthogonalization. *Journal of the Royal Statistical Society. Series C (Applied Statistics)*, 20 (3), 335–338.

Conrad, C., *et al.*, 2010. Per-Field Irrigated Crop Classification in Arid Central Asia Using SPOT and ASTER Data. *Remote Sensing*, 2 (4), 1035–1056.

Corcoran, P., Winstanley, A., and Mooney, P., 2010. Segmentation performance evaluation for object-based remotely sensed image analysis. *International Journal of Remote Sensing*, 31 (3), 617–645.

Costa, G., *et al.*, 2008. Genetic adaptation of segmentation parameters. *In*: T. Blaschke, S. Lang and G. Hay, eds. *Object-Based Image Analysis. Spatial Concepts for Knowledge-Driven Remote Sensing Applications*. Springer, 679–695.

De Kok, R., 2012. Spectral Difference in the Image Domain for Large Neighborhoods, a GEOBIA Pre-Processing Step for High Resolution Imagery. *Remote Sensing*, 4 (8), 2294–2313.

DEFINIENS, 2004. *eCognition 4. User Guide*. DEFINIENS.

DEFINIENS, 2008. *Definiens Developer 7. User Guide*. DEFINIENS.

Delves, L., *et al.*, 1992. Comparing the performance of SAR image segmentation algorithms. *International Journal of Remote Sensing*, 13 (11), 2121–2149.

Dragut, L., Tiede, D., and Levick, S., 2010. ESP: a tool to estimate scale parameter for multiresolution image segmentation of remotely sensed data. *International Journal of Geographical Information Science*.

Esch, T., *et al.*, 2008. Improvement of Image Segmentation Accuracy Based on Multiscale Optimization Procedure. *IEEE Geoscience and Remote Sensing Letters*, 5 (3), 463–467.

Espindola, G., *et al.*, 2006. Parameter selection for region-growing image segmentation algorithms using spatial autocorrelation. *International Journal of Remote Sensing*, 27 (14), 3035–3040.

Farebrother, R., 1974. Algorithm AS 79: Gram-Schmidt Regression. *Journal of the Royal Statistical Society. Series C (Applied Statistics)*, 23 (3), 470–476.

Fotheringham, A., Brundson, C., and Charlton, M., 2000. *Quantitative Geography: Perspectives on Spatial Data Analysis*. Sage Publications.

Fu, G., *et al.*, 2013. Segmentation for High-Resolution Optical Remote Sensing Imagery Using Improved Quadtree and Region Adjacency Graph Technique. *Remote Sensing*, 5 (7), 3259–3279.

Gao, H., 2009. *Digital Analysis of Remotely Sensed Imagery*. McGraw-Hill.

Gao, Y., Kerle, N., and Mas, J.F., 2009. Object-based image analysis for coal fire-related

land cover mapping in coal mining areas. *Geocarto International*, 24 (1), 25–36.

Gao, Y., *et al.*, 2011. Object-based classification with features extracted by a semi-automatic feature extraction algorithm - SEaTH. *Geocarto International*, 26 (3), 211–226.

Geary, R., 1954. The Contiguity Ratio and Statistical Mapping. *The Incorporated Statistician*, 5 (3), 115–145.

Hay, G. and Castilla, G., 2008. Geographic Object-Based Image Analysis (GEOBIA): A new name for a new discipline. *In*: T. Blaschke, S. Lang and G. Hay, eds. *Object-Based Image Analysis. Spatial Concepts for Knowledge-Driven Remote Sensing Applications*. Springer, 75–89.

Hermosilla Gómez, T., 2011. Detección automática de edificios y clasificación de usos del suelo en entornos urbanos con imágenes de alta resolución y datos LiDAR. Thesis (PhD). Universidad Politécnica de Valencia.

Johnson, B. and Xie, Z., 2011. Unsupervised image segmentation evaluation and refinement using a multi-scale approach. *ISPRS Journal of Photogrammetry and Remote Sensing*, 66, 473–483.

Jyothi, B., Babu, G., and Krishna, I., 2008. Object Oriented and Multi-Scale Image Analysis: Strengths, Weaknesses, Opportunities and Threats-A Review. *Journal of Computer Science*, 4 (9), 706–712.

Kim, M., Madden, M., and Warner, T., 2008. Estimation of optimal size for the segmentation of forest stands with multispectral IKONOS imagery. *In*: T. Blaschke, S. Lang and G. Hay, eds. *Object-Based Image Analysis. Spatial Concepts for Knowledge-Driven Remote Sensing Applications*. Springer, 291–307.

Lang, S., 2008. Object-based image analysis for remote sensing applications: modeling reality - dealing with complexity. *In*: T. Blaschke, S. Lang and G. Hay, eds. *Object-Based Image Analysis. Spatial Concepts for Knowledge-Driven Remote Sensing Applications*. Springer, 3–27.

Liua, D. and Xiab, F., 2010. Assessing object-based classification: advantages and limitations. *Remote Sensing Letters*, 1 (4), 187–194.

Lu, D. and Weng, Q., 2007. A survey of image classification methods and techniques for improving classification performance. *International Journal of Remote Sensing*, 28 (5), 823–870.

Lucieer, A., 2004. Uncertainties in Segmentation and their Visualisation. Thesis (PhD). Universiteit Utrecht.

Lucieer, A. and Stein, A., 2002. Existential Uncertainty of Spatial Objects Segmented From Satellite Sensor Imagery.. *IEEE Transactions on Geoscience and Remote Sensing.*, 40(11), 25182521.

Marpu, P., 2009. Geographic Object-based Image Analysis. Thesis (PhD). Techniche Universität Bergakademie Freiberg.

Möller, M., Lymburner, L., and Volk, M., 2007. The comparison index: A tool for assessing the accuracy of image segmentation. *International Journal of Applied Earth Observation and Geoinformation*, 9-3, 311–321.

Myint, S.W., *et al.*, 2013. Object vs. pixel: a systematic evaluation in urban environments. *Geocarto International*, 28 (7), 657–678.

Neubert, M. and Herold, H., 2008. Assessment of remote sensing image segmentation quality. *In*: *International Archives of Photogrammetry, Remote Sensing and Spatial Information Sciences*, Vol. XXXVIII-4/C1.

Neubert, M., Herold, H., and Meinel, G., 2008. Assessing image segmentation quality-concepts, methods and application. *In*: T. Blaschke, S. Lang and G. Hay, eds. *Object-*

Based Image Analysis. Spatial Concepts for Knowledge-Driven Remote Sensing Applications. Springer, 769–784.

Neubert, M. and Meinel, G., 2003. Evaluation of Segmentation Programs for High Resolution Remote Sensing Applications. *In*: M. Schroeder, K. Jacobsen and C. Heipke, eds. *Procedings of the Joint ISPRS/EARSeL Workshop "High Resolution Mapping from Space 2003"*, 6-8 Octubre., Hannover, Germany.

Nussbaum, S. and Menz, G., 2008. *Object-Based Image Analysis and Treaty Verification*. Springer.

Platt, R. and Rapoza, L., 2008. An Evaluation of an Object-Oriented Paradigm for Land Use/Land Cover Classification. *The Proffesional Geographer*, 60 (1), 87–100.

R Development Core Team, 2009. *R: A language and environment for statistical computing*. R Foundation for Statistical Computing.

Radoux, J. and Defourny, P., 2007. A quantitative assessment of boundaries in automated forest stand delineation using very high resolution imagery. *Remote Sensing of Environment*, 110, 468 –475.

Radoux, J. and Defourny, P., 2008. Quality assessment of segmentation results devoted to object-based classification. *In*: T. Blaschke, S. Lang and G. Hay, eds. *Object-Based Image Analysis. Spatial Concepts for Knowledge-Driven Remote Sensing Applications*. Springer, 257–271.

Recio Recio, J., 2009. Técnicas de extracción de características y clasificación de imágenes orientada a objetos aplicadas a la actualización de bases de datos de ocupación del suelo. Thesis (PhD). Universidad Politécnica de Valencia.

Reikik, A., *et al.*, 2007. Review of satellite image segmentation for an optimal fusion system based on the edge and region approaches. *International Journal of Computer Science and Network Security*, 7 (10), 242–250.

Rosa, M.F. and Stow, D.A., 2014. Mapping fuels at the wildland-urban interface using colour ortho-images and LiDAR data. *Geocarto International*, 29 (5), 570–588.

Schiewe, J., 2002. Segmentation of Higth-Resolution remotely sensed Data-Concepts, Applications and Problems. *In*: *Symposium on Geospatial Theory, Processing Applications*, 9-12 July., Ottawa.

Schöpfer, E., Lang, S., and Albrecht, F., 2008. Object-fate analysis: Spatial relationships for the assessment of object transition and correspondence. *In*: T. Blaschke, S. Lang and G. Hay, eds. *Object-Based Image Analysis. Spatial Concepts for Knowledge-Driven Remote Sensing Applications*. Springer, 785–801.

Smith, G., 2008. The development of integrated object-based analysis of EO data within UK national land cover products. *In*: T. Blaschke, S. Lang and G. Hay, eds. *Object-Based Image Analysis. Spatial Concepts for Knowledge-Driven Remote Sensing Applications*. Springer, 513–528.

Tian, J. and Chen, D., 2007. Optimization in multi-scale segmentation of high-resolution satellite images for artificial feature recognition. *International Journal of Remote Sensing*, 28 (20), 4625–4644.

Tzotsos, A., Iosifidis, C., and Argialas, D., 2008. A hybrid texture-based and region-based multi-scale image segmentation algorithm. *In*: T. Blaschke, S. Lang and G. Hay, eds. *Object-Based Image Analysis. Spatial Concepts for Knowledge-Driven Remote Sensing Applications*. Springer, 221–236.

Walker, J. and Blaschke, T., 2008. Object-based land-cover classification for the Phoneix metropolitan area: optimization vs. transportability. *International Journal of Remote Sensing*, 29 (7), 2021–2040.

Woodcock, C. and Strahler, A., 1987. The Factor of Scale in Remote Sensing. *Remote*

Sensing of Environment, 21, 311–332.

Yan, G., *et al.*, 2006. Comparison of pixel-based and object-oriented image classification approaches-a case study in a coal fire area, Wuda, Inner Mongolia, China. *International Journal of Remote Sensing*, 27 (18), 4039–4055.

Yu, Q., *et al.*, 2006. Object-based Detailed Vegetation Classification with Airborne High Spatial Resolution Remote Sensing Imagery. *Photogrammetric Engineering & Remote Sensing*, 72 (7), 799–811.

Zabala, A., Cea, C., and Pons, X., 2010. Segmentation and thematic classification of color orthophotos over non-compressed and JPEG 2000 compressed images. *In*: *ISPRS Archives*, Vol. XXXVIII-4/C7, 29 June - 2 July., Ghent, Belgium.

Zhang, C. and Xie, Z., 2014. Data fusion and classifier ensemble techniques for vegetation mapping in the coastal Everglades. *Geocarto International*, 29 (3), 228–243.

Zhang, H., Fritts, J., and Goldman, S., 2005. A Co-evaluation Framework for Improving Segmentation Evaluation. *Proc. SPIESignal Processing, Sensor Fusion and Target Recognition.*

Zhang, H., Fritts, J., and Goldman, S., 2008. Image segmentation evaluation: A survey of unsupervised methods. *Computer Vision and Image Understanding*, 110, 260–280.

Zhang, Y., 1996. A Survey on Evaluation Methods for Image Segmentation. *Pattern Recognition*, 29 (8), 1335–1346.

Zhou, W., *et al.*, 2009. Object-based land cover classification of shaded areas in high spatial resolution imagery of urban areas: A comparison study. *Remote Sensing of Environment*, 113, 1769–1777.

Table 1. Medians of the scale parameter and p-values of the Fisher exact test when comparing the scale parameter distribution of two different land uses.

Land cover	**med. SP**	**R.c.**	**I.c.**	**I.f.t.**	**A.l.**	**O.t.**	**G.**	**S.**
Almond trees	300	0.0056	0.0026	0.0022	0.215	0.2675	0.025	0.0002
Rainfed cereal	300		0.1096	0.1166	0.006	0.4201	0.0794	0.0006
Irrigated cereal	375			0.0022	0.1682	0.2553	0.9072	0.0002
Irr. fruit trees	250				0.0002	0.0092	0.0068	0.0166
Arable land	350					0.0282	0.0894	0.0002
Olive trees	350						0.2681	0.0002
Greenhouses	350							0.0002
Seedlings	250							

Table 2. Medians of $\overline{\text{Diff}}$ calculated with the reflectivity in the red band with the global and local approach and p-values of the Man-Whitney U test to compare both medians.

Land cover	**med. $\overline{\text{Diff}}$ global**	**med. $\overline{\text{Diff}}$ local**	**med. $\overline{\text{Diff}}$ p-value**
Almond trees	3,621.7	4,454.5	6.413×10^{-158}
Rainfed cereal	1,800.7	2,193.1	1.096×10^{-121}
Irrigated cereal	1,382.9	2,835.7	0
Irrigated fruit trees	3,331.8	3,444.5	0.137
Arable land	1,121.1	2,216.0	0
Olive trees	4,354.4	4,783.7	2.093×10^{-24}
Greenhouses	4,419.8	4,402.9	0.492
Seedlings	2,585.5	2,869.5	1.8×10^{-29}

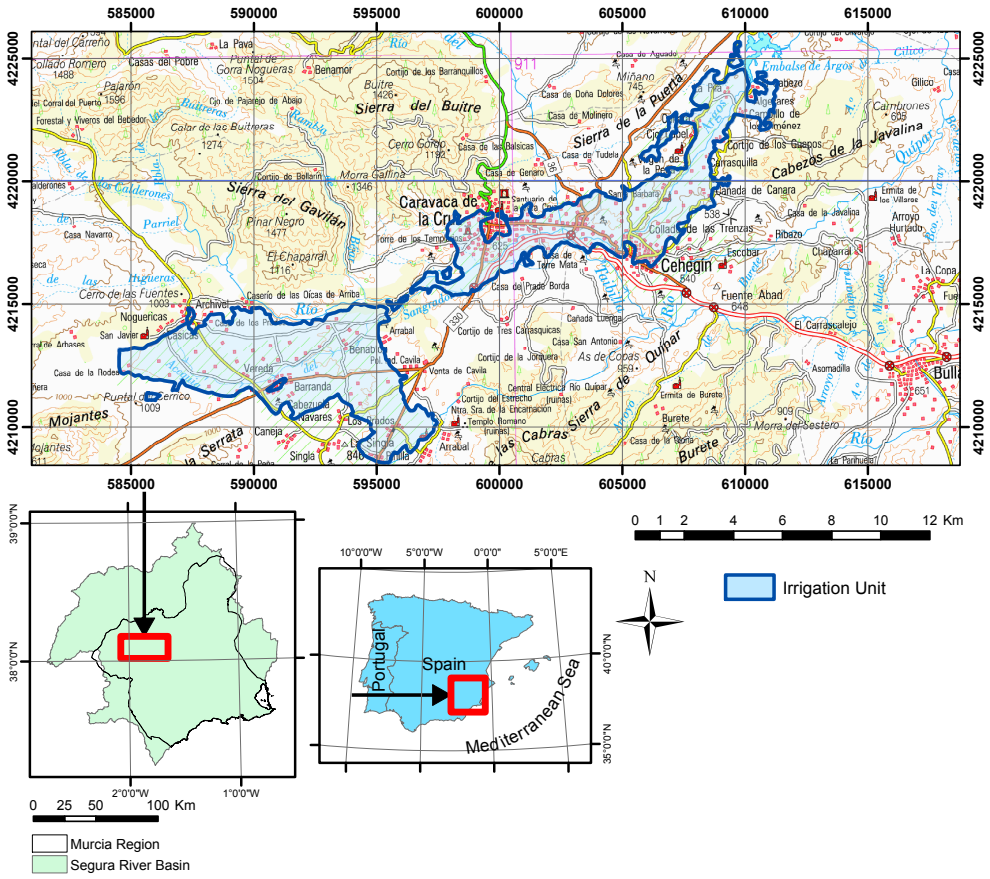

Figure 1. Irrigation Unit n^o 28. National Topographic Map 1:200,000 from the Spanish National Geographic Institute (IGN).

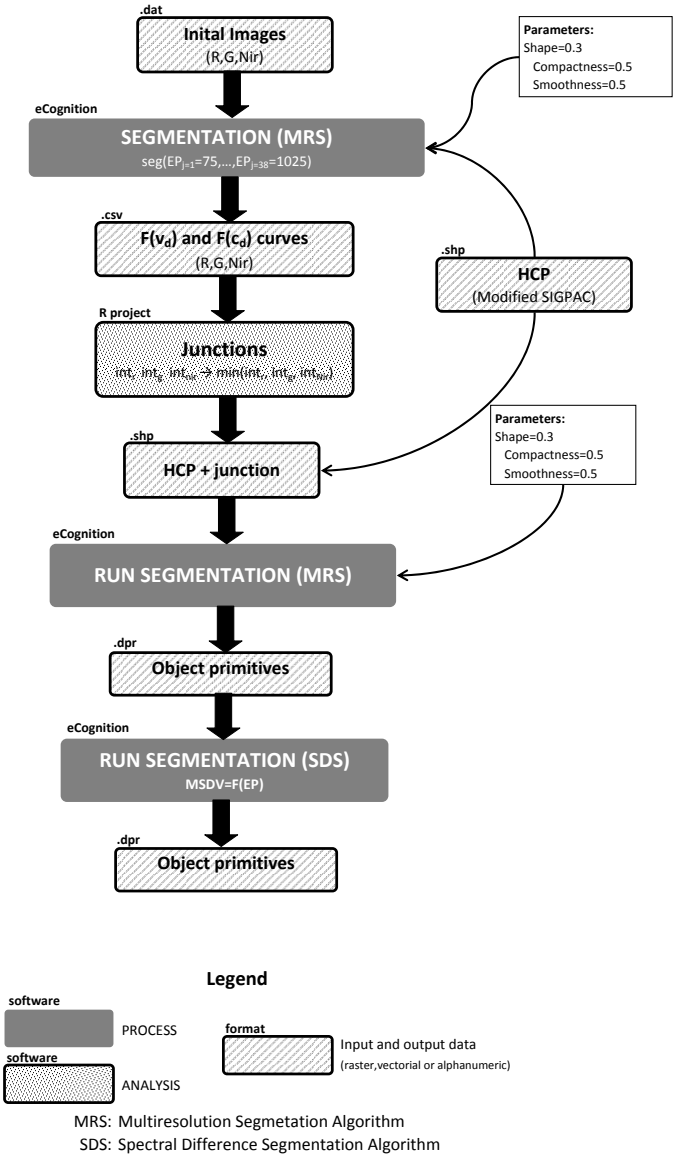

Figure 2. Work flow.

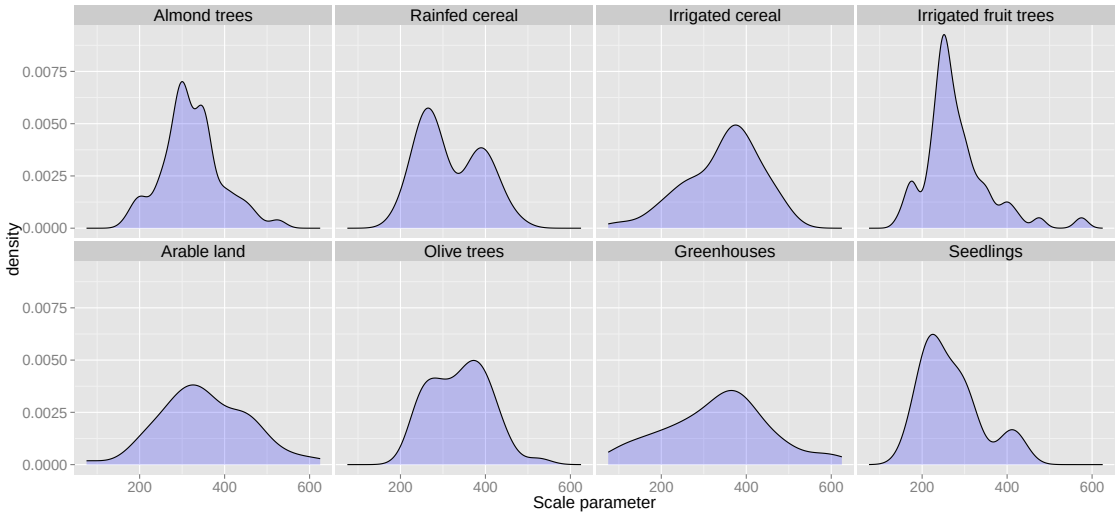

Figure 3. Scale parameter distribution along the different classes.

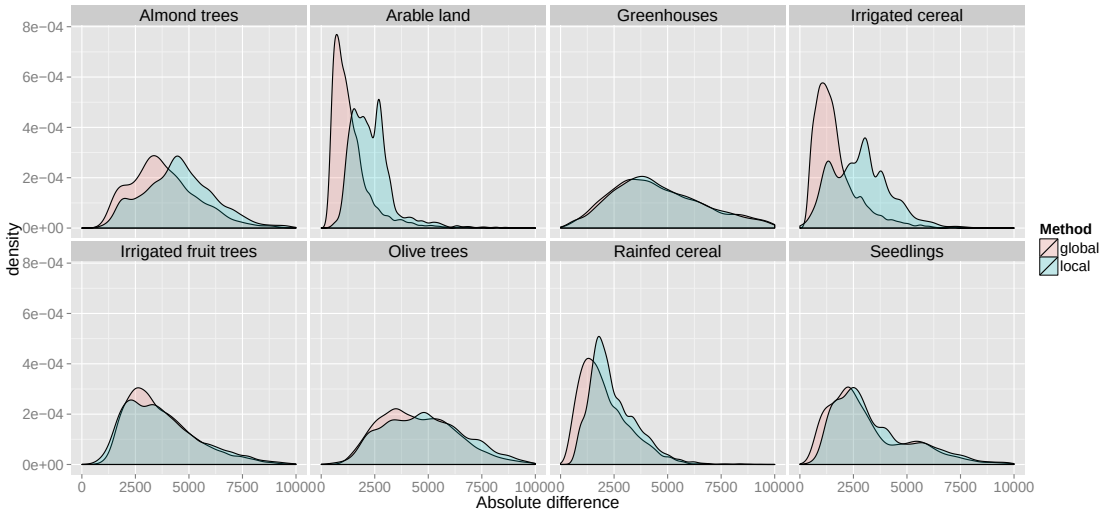

Figure 4. Comparison of the distribution of the parameter average difference, using local an global approach, in all the land uses.

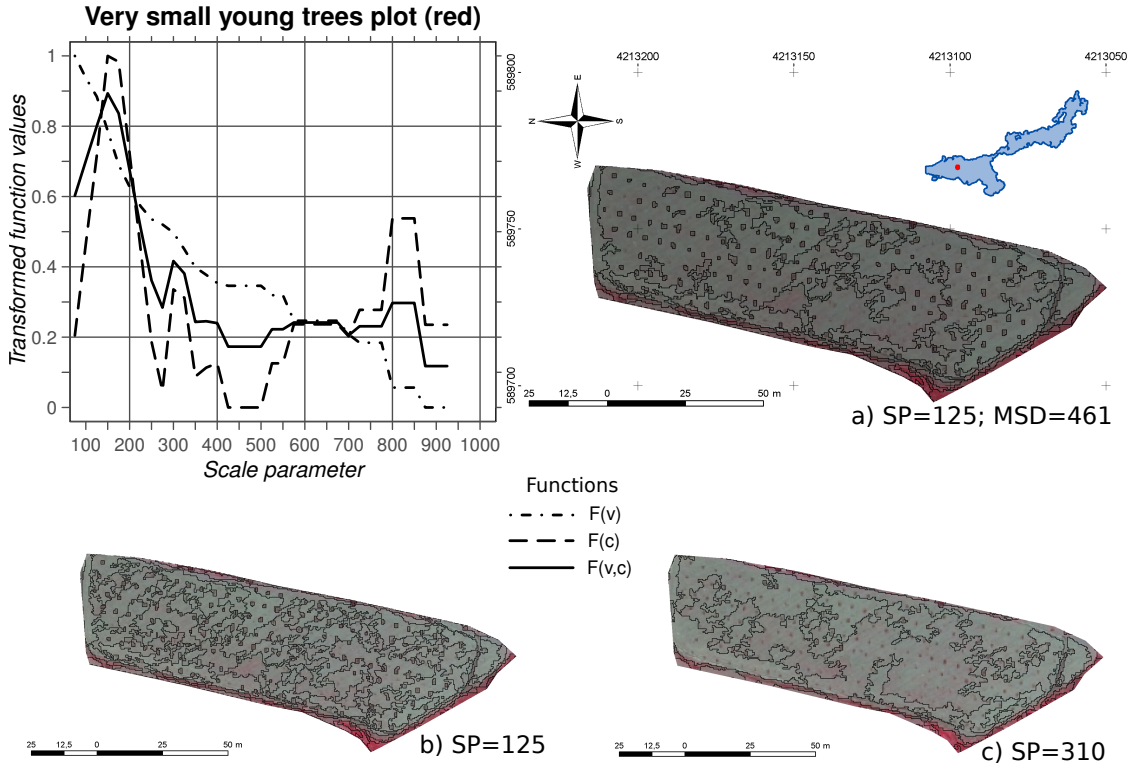

Figure 5. F(v), F(c) and F(v,c) curves in an homogeneous plot with small trees (0.696 ha). Applying the entire methodology with SP=125 and MSD=461 (a) . Applying just the scale parameter optimization with SP=125 (b) . Applying Espindola methodology with a global SP=310 (c).

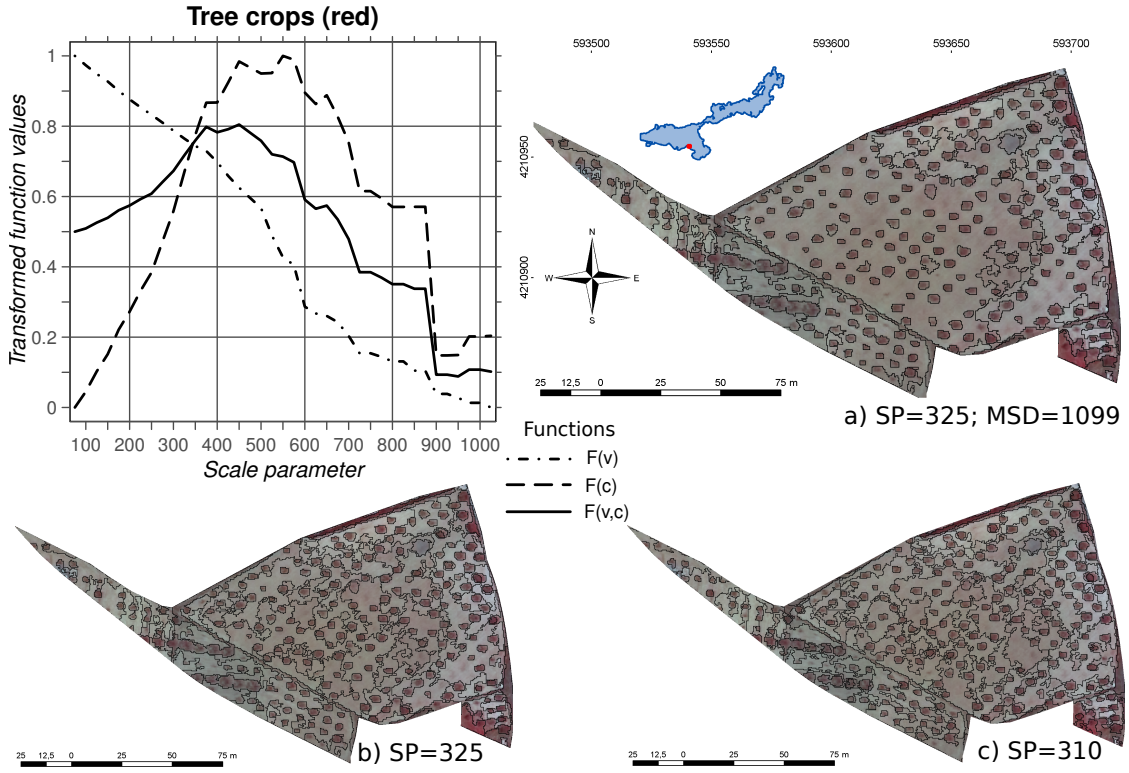

Figure 6. F(v), F(c) and F(v,c) in an almond trees plot with low density and without irrigation (1.621 ha). In this kind of plot our approach works very well, especially if the plots are large and with only one type of land cover. Results obtained after the application of the entire methodology with SP=325 and MSD=1099 (a). Applying just the optimization of the scale parameter with SP=325 (b). Applying Espindola methodology with a global SP=310 (c).

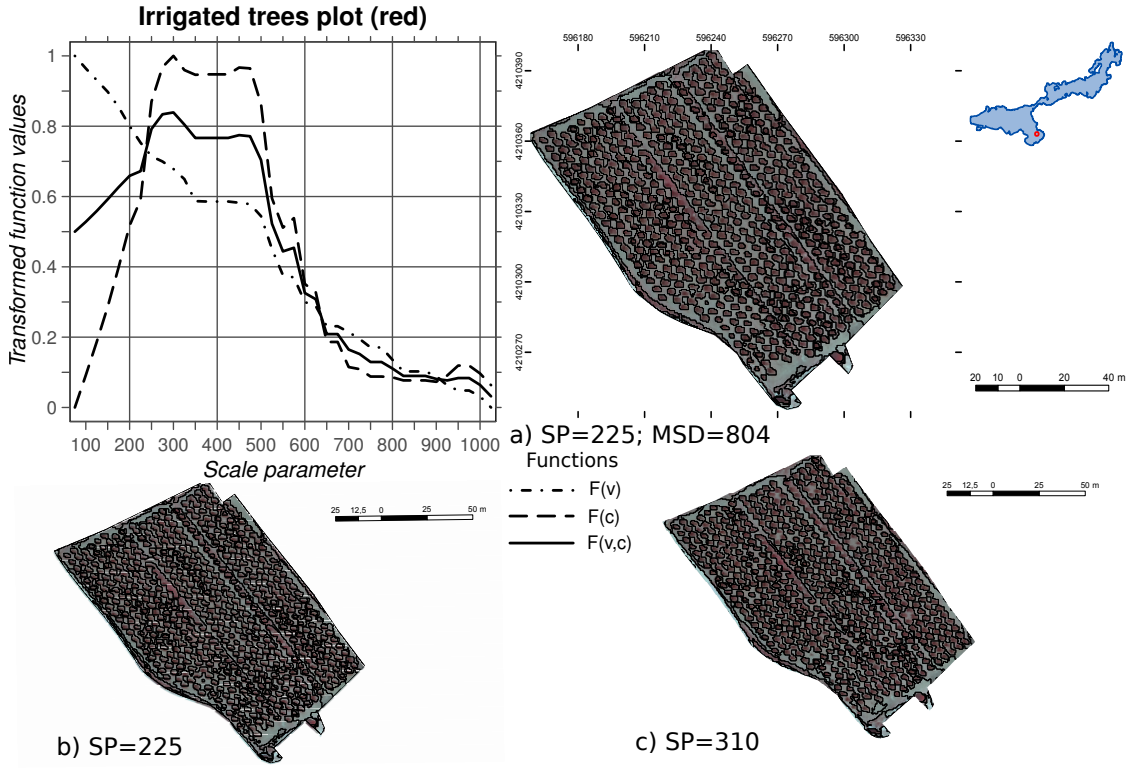

Figure 7. F(v), F(c) and F(v,c) curves for the red band in a irrigated fruit-trees plot (1.332 ha). The curves shows the uncertainty in the estimation of the scale parameter that maximizes the average curve when the slope of such curve is very small. The intersection criterion is less uncertain. Results obtained after the application of the entire methodology with SP=225 and MSD=804 (a). Applying just the optimization of the scale parameter with SP=225 (b). Applying Espindola methodology with a global SP=310 (c).

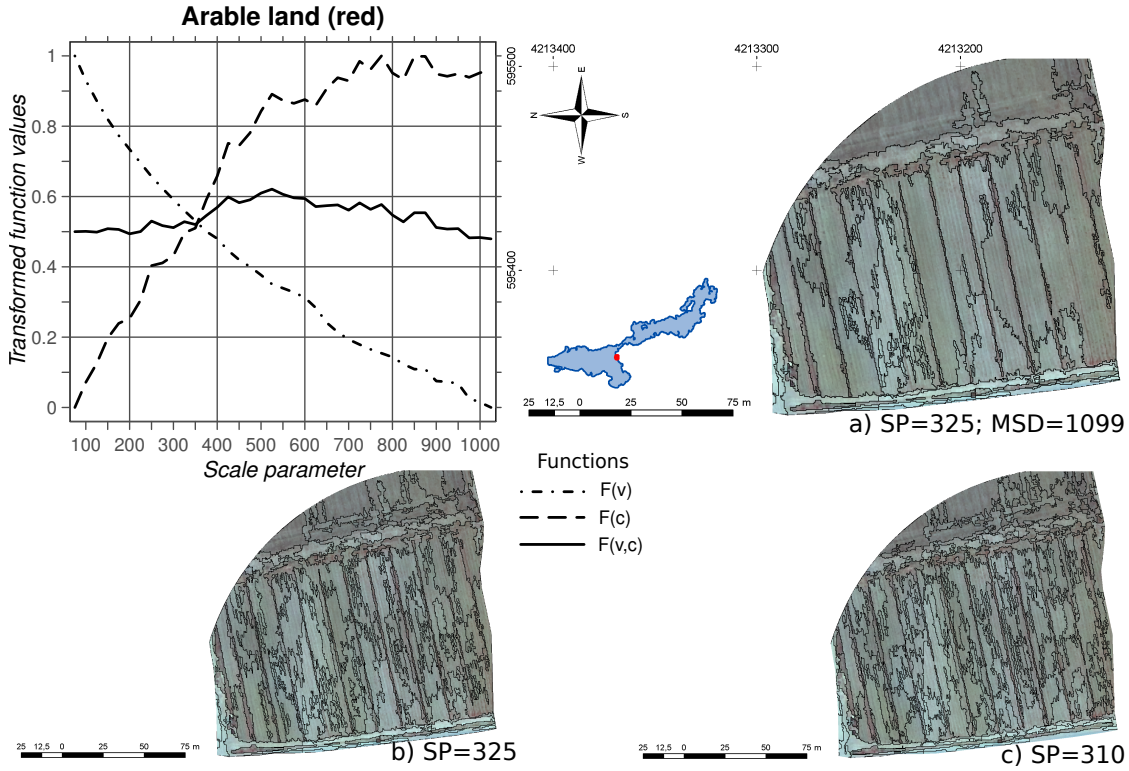

Figure 8. F(v), F(c) and F(v,c) curves for the red band in a ploughed plot (2.453 ha). In this kind of very homogeneous plots, optimisation is less relevant because almost any scale parameter lower than 300 would have an acceptable result. Results obtained after the application of the entire methodology with SP=325 and MSD=1099 (a). Applying just the optimization of the scale parameter with SP=325 (b). Applying Espindola methodology with a global SP=310 (c).

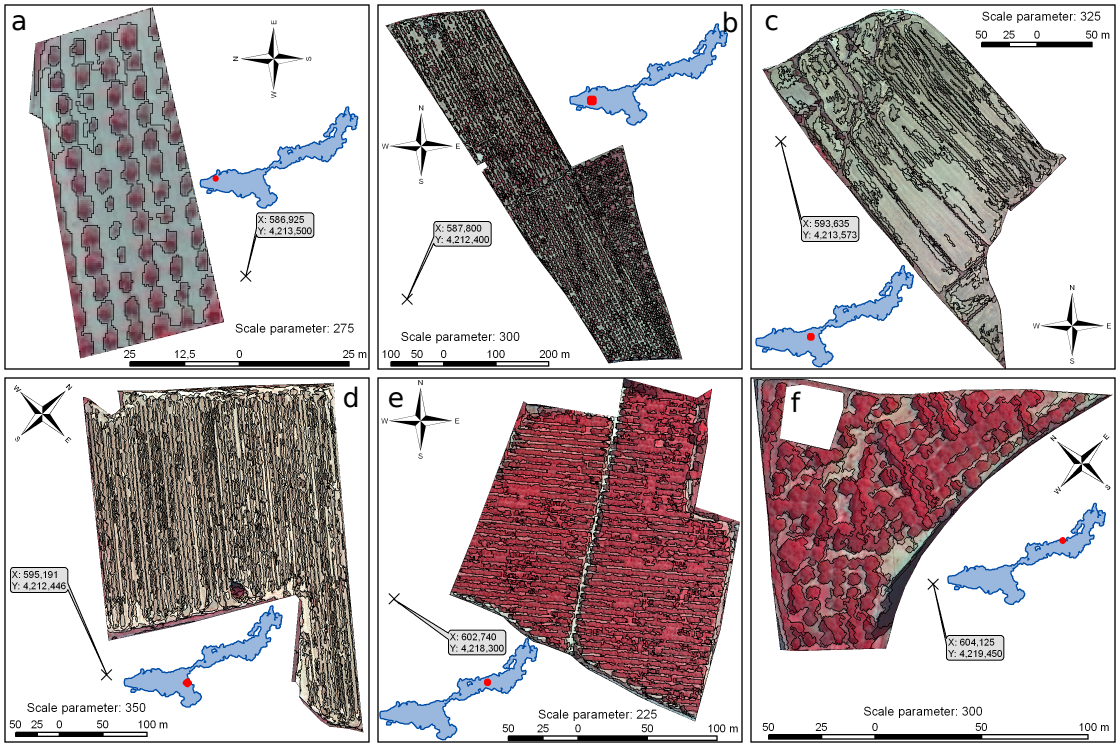

Figure 9. Examples of the results obtained with the proposed segmentation method: Two almond tree plots, a small one (a) and a large one (b); two cereal plots (c and d); and two irrigation plots with fruit trees showing the overlapping between canopies (e, f). Surfaces are a: 0.233 ha, b: 13.529 ha, c: 3.945 ha, d: 8.259 ha, e: 3.237 ha and f: 1.088 ha.

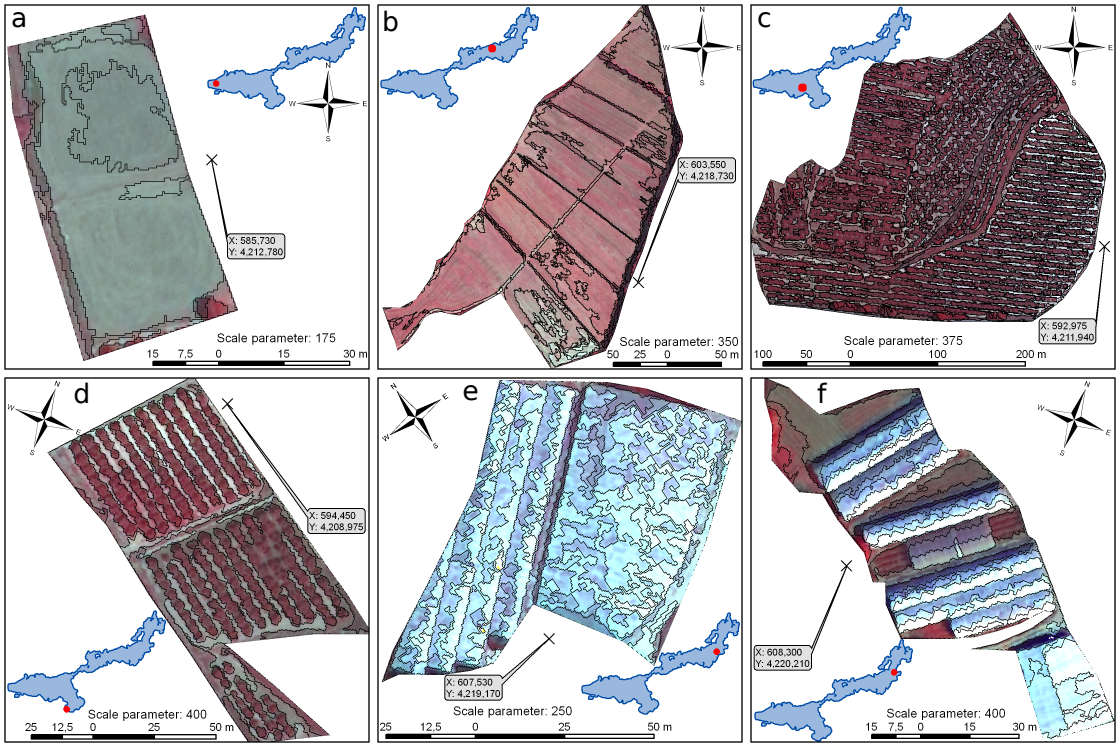

Figure 10. Examples of the results obtained with the proposed segmentation method: Two arable land plots, a small one (a) and a large one (b); two olive tree plots (c and d); and two groups of greenhouses (e and f). Surfaces are a: 0.257 ha, b: 4.209 ha, c: 9.721 ha, d: 0.838 ha, e: 0.514 ha and f: 0.466 ha.